

# Electrical Response of Poly(*N*-[3-(dimethylamino)Propyl] Methacrylamide) to CO<sub>2</sub> at a Long Exposure Period

Zahra Shahrababaki, Farshad Oveissi, Syamak Farajikhah, Mohammad B. Ghasemian, Ross D. Jansen-van Vuuren, Philip G. Jessop, Jimmy Yun, Fariba Dehghani,\* and Sina Naficy\*



Cite This: *ACS Omega* 2022, 7, 22232–22243



Read Online

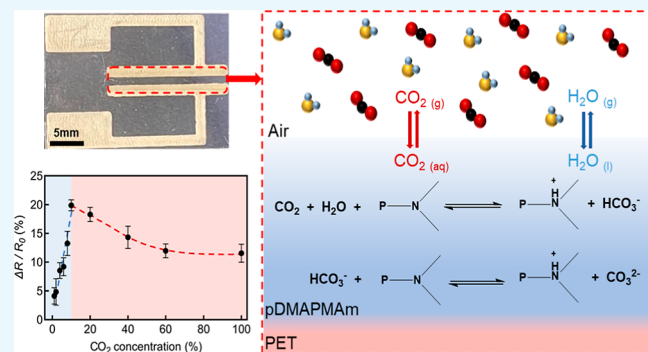
ACCESS |

Metrics & More

Article Recommendations

Supporting Information

**ABSTRACT:** Amine-functionalized polymers (AFPs) are able to react with carbon dioxide (CO<sub>2</sub>) and are therefore useful in CO<sub>2</sub> capture and sensing. To develop AFP-based CO<sub>2</sub> sensors, it is critical to examine their electrical responses to CO<sub>2</sub> over long periods of time, so that the device can be used consistently for measuring CO<sub>2</sub> concentration. To this end, we synthesized poly(*N*-[3-(dimethylamino)propyl] methacrylamide) (pDMAPMAM) by free radical polymerization and tested its ability to behave as a CO<sub>2</sub>-responsive polymer in a transducer. The electrical response of this polymer to CO<sub>2</sub> upon long exposure times was measured in both the aqueous and solid phases. Direct current resistance measurement tests on pDMAPMAM films printed along with the silver electrodes in the presence of CO<sub>2</sub> at various concentrations reveal a two-region electrical response. Upon continuous exposure to different CO<sub>2</sub> flow rates (at a constant pressure of 0.2 MPa), the resistance first decreased over time, reaching a minimum, followed by a gradual increase with further exposure to CO<sub>2</sub>. A similar trend is observed when CO<sub>2</sub> is introduced to an aqueous solution of pDMAPMAM. The in situ monitoring of pH suggests that the change in resistance of pDMAPMAM can be attributed to the protonation of tertiary amine groups in the presence of CO<sub>2</sub>. This two-region response of pDMAPMAM is based on a proton-hopping mechanism and a change in the number of free amines when pDMAPMAM is exposed to various levels of CO<sub>2</sub>.



## INTRODUCTION

Carbon dioxide (CO<sub>2</sub>) detectors are used in a variety of applications<sup>1</sup> and are being explored with novel materials to suit a range of contexts including medical,<sup>2</sup> air quality monitoring,<sup>3</sup> marine and environmental,<sup>4</sup> fire detection,<sup>5</sup> and smart food packaging.<sup>6,7</sup> Conventionally, CO<sub>2</sub> is detected via fluorescence,<sup>8</sup> gas chromatography,<sup>9</sup> and infrared spectrometry.<sup>10</sup> Although these detection methods are highly selective and sensitive, the instrumentation used is typically bulky, requires a large power supply during operation, and is relatively expensive,<sup>11</sup> limiting their more widespread use in everyday applications, for example, in situ food monitoring.<sup>12</sup> Thus, there is a demand for miniaturized, easy-to-implement, low-power, and inexpensive CO<sub>2</sub> sensors.

To date, colorimetric<sup>13</sup> and potentiometric<sup>7,14</sup> techniques are among the most promising methods for CO<sub>2</sub> detection. Although colorimetric CO<sub>2</sub> indicators are simple, require low power, and are convenient to use, they are qualitative or, at best, semi-quantitative, and the color change observed is subjective.<sup>15</sup> Potentiometric CO<sub>2</sub> sensors are low-cost, have high selectivity, and can continuously monitor the concentration of the CO<sub>2</sub> gas; however, they often operate at high temperatures (above 400 °C) and require connection to an

external power source (e.g., a battery), hindering their potential for use in untethered applications.<sup>7</sup>

An alternative to the above methods is to employ a battery-less CO<sub>2</sub>-responsive polymer-based sensor. This type of sensor works based on the change in electrical properties (conductivity and dielectric permittivity) of a CO<sub>2</sub>-responsive polymer upon absorption and desorption of CO<sub>2</sub> molecules by the polymer.<sup>16</sup> The CO<sub>2</sub> desorption can be initiated by purging with an inert gas such as nitrogen or by mild heating.<sup>17,18</sup>

Amidines,<sup>19,20</sup> guanidines,<sup>21,22</sup> and amines<sup>23,24</sup> are commonly used as CO<sub>2</sub>-responsive functional groups in CO<sub>2</sub>-responsive polymers.<sup>25</sup> Tertiary amines have many advantages over other CO<sub>2</sub>-responsive functional groups. For example, the synthesis of CO<sub>2</sub>-switchable polymers possessing tertiary amine groups is relatively simpler than those possessing amidine and guanidine groups.<sup>25</sup> The CO<sub>2</sub>-responsivity of the

Received: February 14, 2022

Accepted: June 8, 2022

Published: June 22, 2022



polymers is due to the transition from an unprotonated to a protonated state when exposed to CO<sub>2</sub> (and vice versa when CO<sub>2</sub> is removed).<sup>25</sup> The nature of this transition depends on the pK<sub>aH</sub> of the functional groups, where pK<sub>aH</sub> is the basicity of the polymer, essentially equivalent to the pK<sub>a</sub> of the protonated compound.<sup>26</sup> Although a higher pK<sub>aH</sub> produces a higher degree of protonation (DOP), CO<sub>2</sub> desorption occurs with more difficulty.<sup>25</sup> For example, amidine is a weak base (pK<sub>aH</sub> = 5.4) with a low DOP,<sup>19</sup> while guanidine is a super base (pK<sub>aH</sub> = 13.5) that is difficult to deprotonate.<sup>21</sup> However, tertiary amine groups are moderate bases (pK<sub>aH</sub> = 6–7), resulting in good switchability (easy to protonate and have good reversibility) compared to amidine and guanidine groups.<sup>26</sup> Of the many amine-functionalized polymers (AFPs), polyethyleneimine (PEI),<sup>27,28</sup> poly(*N,N*-dimethylaminoethyl methacrylate) (pDMAEMA),<sup>29–31</sup> and poly(*N,N*-diethylaminoethyl methacrylate) (pDEAEMA)<sup>30,32</sup> have been explored for CO<sub>2</sub> detection. For example, Han et al. recently reported a PEI-functionalized carbon nanotube thin-film sensor capable of CO<sub>2</sub> detection at room temperature, which works based on the acid-base interaction between CO<sub>2</sub> molecules and amine groups of PEI.<sup>27</sup> In another example, microgels consisting of pDMAEMA/SiO<sub>2</sub> and a shell of polyetheramine were used for adsorption and determination of CO<sub>2</sub> at 25 °C under different pressures.<sup>29</sup> Similarly, a random copolymer of DEAEMA and acrylamide acrylonitrile repeat units was used for sensing CO<sub>2</sub> in aqueous solutions.<sup>33</sup> It should be noted that certain AFPs, for example, pDMAEMA and pDEAEMA, can experience a low extent of protonation and the formation of products such as methacrylic acid as a consequence of monomer hydrolysis during polymerization due to their low pK<sub>aH</sub> values compared to amidines, all of which affect CO<sub>2</sub>-switchability.<sup>34</sup> pDMAPMAM is a CO<sub>2</sub>-responsive polymer containing tertiary amine groups in the side chain which is readily prepared from the commercially available and inexpensive monomer, *N*-[3-(dimethylamino)propyl]-methacrylamide (DMAPMAM). DMAPMAM is hydrolytically stable as it possesses amide linkages rather than amidine or ester groups.<sup>34</sup> Additionally, unlike primary and secondary amines, the tertiary amine group on DMAPMAM can only react with CO<sub>2</sub> in the presence of water. It has been shown that in the presence of water, pDMAPMAM exhibits CO<sub>2</sub> absorption properties and a higher pK<sub>aH</sub> value (8.8) compared to other available amine-based polymers such as pDMAEMA (pK<sub>aH</sub> = 7–7.5) and pDEAEMA (pK<sub>aH</sub> = 6.9–7.5). The higher pK<sub>aH</sub> value of pDMAPMAM suggests a relatively greater extent of protonation of pDMAPMAM when CO<sub>2</sub> interacts with the side groups.<sup>34–36</sup>

For many applications, such as in food packaging, it is critical to know how the sensitivity of a sensor changes when it is exposed to CO<sub>2</sub> concentration for an extended time. However, to the best of our knowledge, the effect of long-term exposure to CO<sub>2</sub> on the electrical response of AFPs has been scarcely studied. Most work reporting CO<sub>2</sub> detection by AFP-based sensors focuses on the short-term (5–20 min) impact of CO<sub>2</sub> on the resistance of the polymer, suggesting that the conductivity of the sensing polymer increases in the presence of CO<sub>2</sub>.<sup>37</sup> Doan et al., in contrast, reported an increase in the Direct current (DC) resistance of PEI films as the CO<sub>2</sub> concentration increased from 400 to 10<sup>4</sup> ppm.<sup>38</sup> Thus, there is a need to resolve this tension.

We hypothesized that continuous CO<sub>2</sub> absorption affects the extent of protonation and, consequently, the electrical properties of the polymer over time. Herein, we aim to

understand the mechanism and the effect of long-term exposure of pDMAPMAM to CO<sub>2</sub> on a polymer's electrical response. To this end, pDMAPMAM was synthesized by free radical polymerization, and CO<sub>2</sub> sensors were then prepared via printing for DC resistance measurements. First, we characterized the polymer using size exclusion chromatography (SEC), Fourier-transform infrared spectroscopy (FTIR), proton nuclear magnetic resonance (<sup>1</sup>H NMR), and scanning electron microscopy (SEM). Then, the effect of CO<sub>2</sub> exposure on the pH and resistance of pDMAPMAM solutions with various polymer concentrations was explored. Additionally, we studied the sensitivity of pDMAPMAM in the solid state toward different concentrations of CO<sub>2</sub> via CO<sub>2</sub>-dependent DC resistance measurements. A quartz crystal microbalance (QCM) was used to demonstrate the CO<sub>2</sub> absorption and desorption of pDMAPMAM in the solid state. Finally, the behavior of pDMAPMAM in the presence of CO<sub>2</sub> was understood by comparing the results for the polymer in solution versus solid state.

## EXPERIMENTAL SECTION

**Materials.** *N*-[3-(dimethyl amino) propyl] methacrylamide (DMAPMAM; 99%, M<sub>w</sub> = 170.25 g mol<sup>-1</sup>), 2,2'-azobis(2-methylpropionitrile) (AIBN; 0.2 M in toluene, M<sub>w</sub> = 164.21 g mol<sup>-1</sup>), ethanol (>99.5%, M<sub>w</sub> = 46.07 g mol<sup>-1</sup>), *N,N*-dimethylacetamide (DMAc; ≥ 99.9%, M<sub>w</sub> = 87.12 g mol<sup>-1</sup>), chloroform-d1 (CDCl<sub>3</sub>, ≥ 99.8%, M<sub>w</sub> = 120.38 g mol<sup>-1</sup>) l-(+)-lactic acid (80%, M<sub>w</sub> = 90.08 g mol<sup>-1</sup>), and hydrochloric acid solution (HCl; 32 wt % in H<sub>2</sub>O, M<sub>w</sub> = 36.46 g mol<sup>-1</sup>) were purchased from Sigma-Aldrich (Australia) and used as received. The silver ink and the universal transparent polyethylene terephthalate (PET) sheets were purchased from LEED-INK (China) and Amazon (Australia), respectively.

**pDMAPMAM Polymerization.** DMAPMAM (10 mL, 5.5 × 10<sup>-2</sup> mol), AIBN (1.4 mL, 5.5 × 10<sup>-4</sup> mol), and ethanol (5 mL, 8.56 × 10<sup>-2</sup> mol) were added to a glass sealed vial (30 mL) and then incubated at 60 °C for 10 h to complete the free radical polymerization. The polymerization process was carried out under sealed conditions to avoid oxygen contamination. After polymerization, the synthesized polymer was transferred to glass Petri dishes and the remaining ethanol evaporated at room temperature before being stored for further usage. Of note, the same batch of the synthesized polymer was used for all the measurements.

**Sensor Fabrication.** The fabrication of sensors was carried out in two steps commencing with the three-dimensional (3D) printing of electrodes and polymer ink. A configuration of two silver electrodes (1 mm apart) was first printed on the PET substrates using a 3D-Bioplotter (EnvisionTEC, Germany) and these were then stored at 60 °C for 12 h to be cured for further usage. A 20 wt % solution of pDMAPMAM in ethanol was then 3D-printed along with the dried conductive silver electrodes and was kept at room temperature overnight to dry for the solid-state measurements. After drying, the real thickness of the polymer was measured to be 120 μm using a caliper. During printing, the polymer ink was extruded through an 840 μm nozzle at 15 °C, while silver ink was extruded through a 250 μm nozzle at 27 °C. Parameters such as the pressure and speed of printing were optimized at 0.2 bar and 13 mm s<sup>-1</sup> for polymer ink and 3.2 bar and 10 mm s<sup>-1</sup> for silver ink. To explore the homogeneity and uniformity of the

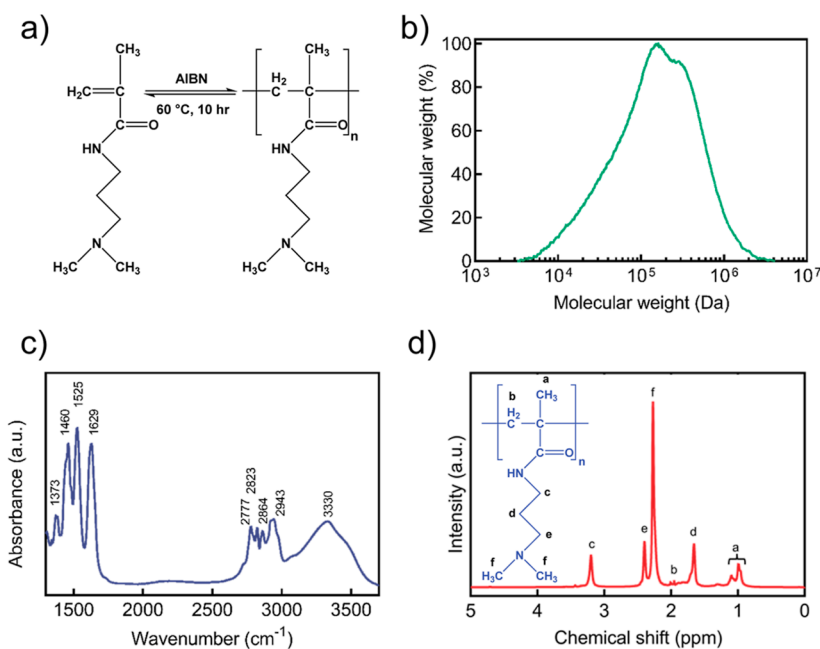


**Figure 1.** pDMAPMAM characterization. (a) Synthesis of pDMAPMAM via free radical polymerization. (b)  $M_w$  distribution from SEC, (c) FTIR, and (d)  $^1\text{H}$  NMR (800 MHz,  $\text{CDCl}_3$ , 25 °C):  $\delta$  0.99–1.10 ppm (d, 3H), 1.66 ppm (s, 2H), 1.95 ppm (s, 2H), 2.27 (s, 6H), 2.40 ppm (s, 2H), and 3.20 ppm (s, 2H).

printed polymer ink, SEM was performed on a JEOL JSM-IT500 system at magnifications of 500, 50, and 20  $\mu\text{m}$ .

**Polymer Characterization.** SEC measurements were performed using a UFC Shimadzu Prominence SEC system with two Phenogel™ columns (5  $\mu\text{m}$ , 104, and 105 Å) running in dimethylacetamide using BHT/LiBr at 0.05 wt % as the eluent at a flow rate of 1 mL min<sup>-1</sup> at 50 °C. The samples were prepared by dissolving pDMAPMAM polymer in the solvent (5–10 mg mL<sup>-1</sup>) and passing the resulting mixture through a 0.45  $\mu\text{m}$  nylon filter before injection. FTIR was performed on a Thermo Scientific Nicolet 6700 spectrometer fitted with an ATR accessory (diamond crystal) at an angle of incidence of 90°. The data were collected at a resolution of 4 cm<sup>-1</sup> over the range of 950–4000 cm<sup>-1</sup> from the average of 32 scans.  $^1\text{H}$  NMR spectroscopy was performed on a Bruker 800 MHz spectrometer using  $\text{CDCl}_3$  as the solvent and 5 mm NMR tubes at room temperature.

**Liquid-State Measurements.** pDMAPMAM solutions of four different concentrations (0.1, 1, 5, and 10 wt %) in deionized water were prepared to study the resistance and pH change of the fabricated polymer in the presence of  $\text{CO}_2$  in the liquid phase. A container of the solution with an inlet for purging  $\text{CO}_2$  (using a glass dispersion tube), a pH meter, and a multimeter (KEITHLY 2450, Textronix, USA) for continuously recording the resistance were used. In the resistance measurement tests, a two-electrode configuration was used in which the electrodes were 1 mm apart. The protonation (%) was calculated based on the following equation

$$\% \text{ protonation} = \frac{[\text{H}^+]}{[\text{H}^+] + K_{\text{aH}}} \times 100\%, [\text{H}^+] = 10^{-\text{pH}}, \\ K_{\text{aH}} = 10^{-8.8} \quad (1)$$

To obtain a better understanding of the pH-based response mechanism of polymer to  $\text{CO}_2$ , different volumes of diluted lactic acid in deionized water (10 vol %) were slowly added to

1 wt % solution of pDMAPMAM in different sets of experiments. Then, the resistance and pH were measured after 2 h. Lactic acid has a high boiling point and was used in this study to protonate the polymer to different protonation levels. Comparing the electrical resistance of polymer solutions protonated by lactic acid with those exposed to  $\text{CO}_2$  could elucidate the role of protonation in the electrical response of the polymer during exposure to  $\text{CO}_2$ .

**Solid-State Measurements.** To measure the resistance change of pDMAPMAM in response to  $\text{CO}_2$  in the solid state, we designed an in-house experimental setup, as shown in Figure S1. The setup consisted of a chamber (a 1 L food container), inlet and outlet ports for purging gas into the chamber, and a RH (relative humidity)-temperature data logger. The fabricated polymer-based sensors were placed inside the chamber containing water and kept in the incubator to humidify the samples ( $\text{RH} \geq 95\%$ , 37 °C, 2 h) as a pre-treatment step. Two mass flow controllers (FMA-2600A Upstream Valve, OMEGA, USA) were installed to control the  $\text{CO}_2$  gas flow rate and adjust the humidity of air in the chamber. Before the introduction of  $\text{CO}_2$  into the chamber, the air was purged for 2 h to maintain the humidity levels and stabilize the polymer's resistance. Then,  $\text{CO}_2$  gas in different concentrations was purged into the test chamber for 2 h. The resistance of pDMAPMAM was continuously measured using a multimeter (KEITHLY 2450, Textronix, USA). The normalized change in electrical resistance ( $\Delta R/R_0$ ) was continuously calculated using the equation:  $\Delta R = R - R_0$ , where  $R_0$  is the initial resistance immediately before the introduction of  $\text{CO}_2$  and  $R$  is the resistance of the sensors. Atomic force microscopy (AFM) and Kelvin probe force microscopy (KPFM) using a Pt-Ir coated tip were carried out on a Bruker Dimension ICON SPM to explore the surface morphology, roughness, and potential of the pDMAPMAM film before and after exposure to  $\text{CO}_2$ . To study the  $\text{CO}_2$  absorption and desorption on pDMAPMAM in the solid state, a QCM200 (Stanford

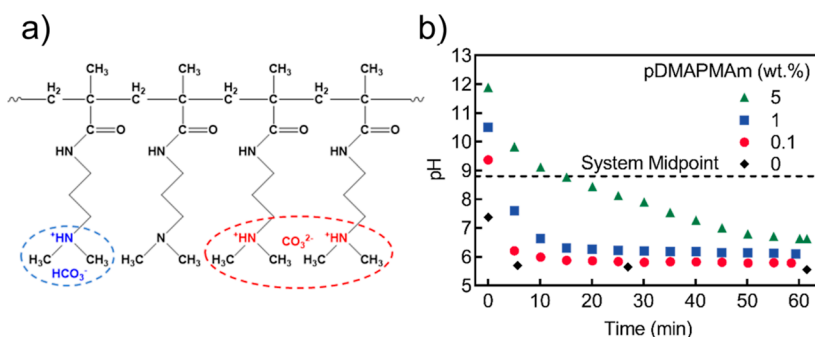


**Figure 2.** pDMAPMAM–CO<sub>2</sub> interaction. (a) Partially protonated state of pDMAPMAM illustrating both neutral and protonated amine sites. (b) pH versus time for different aqueous solutions of pDMAPMAM when exposed to CO<sub>2</sub>.

Research System, USA) was used to demonstrate the mass change at the surface of QCM electrodes. A thin film of pDMAPMAM 20 wt.% solution in ethanol was deposited on the crystals using drop-casting and, after drying, was exposed to the target gases ( $P = 2$  bar). The mass flow rates of N<sub>2</sub> and CO<sub>2</sub> were optimized at 5 mL min<sup>-1</sup> and the gas flow was passed through a water container to be humidified.

To better understand the impact of protonation level on CO<sub>2</sub> detection, a separate experiment was carried out in which 1 M HCl (aq) was added to the pDMAPMAM ink. Then, the pre-treated polymer ink was cast on the interdigitated silver electrodes and dried. Afterward, the sensors were humidified (RH  $\geq$  95%, 37 °C, 2 h), and later the resistance was measured in the presence of CO<sub>2</sub> using the aforementioned setup.

## RESULTS

**Polymer Characterization.** The molecular structure and reaction for the synthesis of pDMAPMAM is shown in Figure 1a. Several characterization methods were carried out that confirm the polymerization took place after 10 h at 60 °C in the presence of the initiator (AIBN). The graph showing the  $M_w$  distribution from SEC in Figure 1b demonstrates a unimodal peak for molecular weight (Mw) distribution of pDMAPMAM as follows:  $M_w = 185$  kDa,  $M_n = 69$  kDa, and PDI ( $M_w/M_n$ ) = 2.7. The synthesized polymer was also characterized using FTIR, and its IR spectrum is shown in Figure 1c. The IR bands are attributed to –CH<sub>3</sub> at 1373 cm<sup>-1</sup>, C–H at 1460 cm<sup>-1</sup>, N–H (amide II) at 1525 cm<sup>-1</sup>, C=O (amide I) at 1629 cm<sup>-1</sup>, –N(CH<sub>3</sub>)<sub>2</sub> at 2777 cm<sup>-1</sup>, –N(CH<sub>3</sub>)<sub>2</sub> at 2823 cm<sup>-1</sup>, C–H at 2864 cm<sup>-1</sup>, C–H at 2943 cm<sup>-1</sup>, and N–H at 3330 cm<sup>-1</sup>.<sup>39,40</sup> The composition of the pDMAPMAM was analyzed using <sup>1</sup>H NMR spectroscopy. As shown in Figure 1d, the characteristic peaks of pDMAPMAM were detected at 0.99–1.10 (a), 1.66 (d), 1.95 (b), 2.27 (f), 2.40 (e), and 3.20 ppm (c).<sup>40</sup>

**pDMAPMAM–CO<sub>2</sub> Interaction in the Aqueous Phase.** In the presence of water, CO<sub>2</sub> protonates the amine groups in AFPs, whereby each protonated amine group becomes associated with an HCO<sub>3</sub><sup>-</sup> (bicarbonate) or a CO<sub>3</sub><sup>2-</sup> (carbonate) counter ion.<sup>25,41</sup> The kinetics of AFP–CO<sub>2</sub> interaction such as pDMAPMAM have been extensively discussed by Jessop group. Alshamrani et al. describe how uncharged basic groups on the CO<sub>2</sub>-responsive species are converted from a neutral state to a protonated cationic state.<sup>26</sup> Since the level of protonation in a polymeric matrix directly impacts its resistance,<sup>42</sup> AFPs can potentially be used in the chemiresistive detection of CO<sub>2</sub>. In the case of pDMAPMAM, for instance, continuous exposure to CO<sub>2</sub> in the presence of

water gradually protonates the tertiary amine side groups of the polymer chains (Figure 2a). While the schematic in Figure 2a illustrates both HCO<sub>3</sub><sup>-</sup> and CO<sub>3</sub><sup>2-</sup>, the dominant species is HCO<sub>3</sub><sup>-</sup>. Since the pH is  $\ll 10$  after CO<sub>2</sub> addition, the formation of carbonate is insignificant. However, if the amount of water is small relative to the amount of amine and the partial pressure is substantially lower than 0.1 MPa, the pH may be  $\gg 10$  and the dominant anion might be carbonate.<sup>26</sup> To correlate the level of protonation of pDMAPMAM with its electrical resistance, the pH and DC resistance of aqueous solutions of pDMAPMAM at various concentrations (0, 0.1, 1, and 5 wt %) were monitored. These solutions were purged with CO<sub>2</sub> at a constant rate of 45 mL min<sup>-1</sup> and a pressure of 0.2 MPa over 60 min. The amount of CO<sub>2</sub> dissolved in aqueous media follows Henry's law, reaching equilibrium under constant temperature and pressure. The introduction of CO<sub>2</sub> to the solutions of pDMAPMAM reduced the overall solution pH regardless of the concentration of the polymer in the solutions (Figure 2b). However, for the 5 wt % polymer solution, this reduction happened slowly due to the higher concentration of amine sites.

In this setup, the system midpoint is defined as the pH at which the number of moles of protonated and unprotonated switchable sites (i.e., tertiary amines) in the system is equal.<sup>43</sup> With this definition, the solution pH in the absence of protonation (before the introduction of CO<sub>2</sub>) commences at a value above the system midpoint, decreasing in the presence of CO<sub>2</sub> as polymer chains are gradually protonated, eventually falling below the midpoint. In contrast, the aqueous-phase midpoint is defined as the pH at which the number of moles of protonated and unprotonated switchable sites in the aqueous phase is equal. For switchable polymers that are completely dissolved in an aqueous solution, the system midpoint and the aqueous-phase midpoint are identical to each other and equal to the  $pK_{aH}$  of the polymer.<sup>43</sup> In the case of dissolved pDMAPMAM, the system midpoint is therefore 8.8.<sup>36</sup> But the system midpoint of solid or incompletely dissolved pDMAPMAM is unknown and most likely depends on the water content.<sup>44</sup>

The conversion of neutral side groups to charged states is representative of the “range of operation” through which the tertiary amine groups in the side chains of the polymers interact with CO<sub>2</sub> via the protonation process. Therefore, to have a wide range of operation, the starting pH of the system should be considerably higher than the system midpoint before CO<sub>2</sub> exposure, with the pH going well below the system midpoint after the exposure to CO<sub>2</sub>.<sup>43</sup> In other words, to have the maximum change in properties caused by an effective

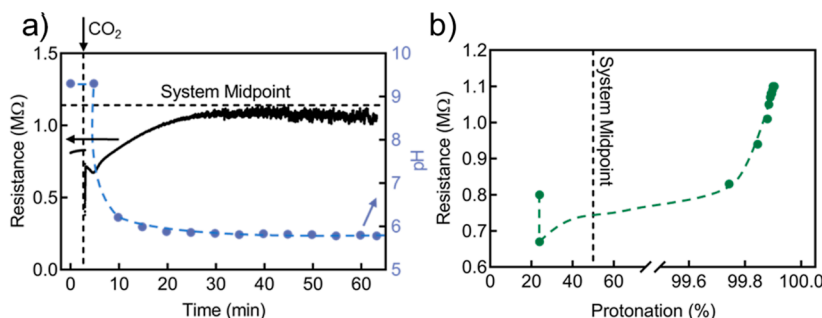


**Figure 3.** Electrical response of pDMAPMAM solutions upon continuous exposure to CO<sub>2</sub>. (a) Resistance and pH of 0.1 wt % pDMAPMAM solution over time. (b) Correlation between resistance and DOP (calculated from eq 1) of 0.1 wt % pDMAPMAM solution.

switching, the CO<sub>2</sub>-switchable polymer should ideally have a very low and very high DOP before and after exposure to CO<sub>2</sub>, respectively. While the system midpoint is determined by the nature of side groups (i.e., the  $pK_{aH}$ ), the starting pH is dictated by the concentration. As expected, the calculation of DOP (eq 1) for pDMAPMAM aqueous solutions with different polymer concentrations (Figure S2) shows that higher pDMAPMAM concentrations lead to lower DOPs prior to CO<sub>2</sub> exposure, for example, 0.08% DOP in 5 wt % pDMAPMAM solution versus 21% DOP in 0.1 wt % pDMAPMAM solution.

The correlation between the DOP of pDMAPMAM and CO<sub>2</sub> exposure was also reflected in the DC resistance of the pDMAPMAM solutions. Figure 3a presents an example of simultaneous measurements of DC resistance and pH for a 0.1 wt % solution, while CO<sub>2</sub> was bubbled at a rate of 45 mL min<sup>-1</sup> for 60 min (data for different concentrations of pDMAPMAM ranging between 0 and 5 wt % are shown in Figure S5b). In this example, the initial resistance was 0.8 MΩ, and the initial pH was 9.3. Once CO<sub>2</sub> was introduced, the resistance sharply decreased for 4 min, reaching a minimum of 0.67 MΩ. The subsequent continuing protonation of pDMAPMAM led to an increase in the resistance from 0.67 to 1.06 MΩ. As expected, the pH of the solution decreased in the presence of CO<sub>2</sub> over time. It should be highlighted that it was not experimentally feasible to record individual pH data points between 9.30 and 6.21 due to its sudden drop. Interestingly, the pH crossed over the system midpoint at around the same time as the DC resistance reached its minimum. The correlation between the DC resistance and DOP (calculated from eq 1) in Figures 3b and S3 further illustrates that the resistance approaches a minimum at around 50% protonation of the tertiary amine side groups of pDMAPMAM.

The observed reduction in resistance immediately after the introduction of CO<sub>2</sub> could have kinetic or thermodynamic origins. Given that CO<sub>2</sub> was bubbled directly into the pDMAPMAM solution, the latter reason for the initial drop in resistance is more plausible. To better elucidate the nature of the correlation between pDMAPMAM's electrical response and protonation, lactic acid was used instead of CO<sub>2</sub> to protonate pDMAPMAM in a batch system. Lactic acid is a high boiling point acid that can similarly protonate pDMAPMAM. Yet, unlike bubbling the polymer solution with CO<sub>2</sub>, where the level of protonation rapidly increases with time, the slow addition of controlled quantities of lactic acid to the polymer solution allows for the elimination of the kinetic contribution. If the observed electrical resistance response of the polymer to

CO<sub>2</sub> (Figure 3b) was due to the protonation of the polymer chains, a similar trend must be seen when protonation is performed in batch experiments with another protonating reagent (i.e., lactic acid). Figure 4 shows the change in

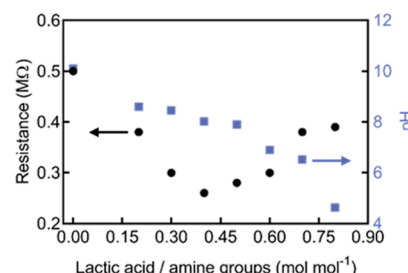


**Figure 4.** Resistance and pH of 1 wt % pDMAPMAM solution protonated with lactic acid 10 vol % vs the molar ratio of lactic acid to amine groups.

resistance and pH of pDMAPMAM solution (1 wt % in deionized water) versus the molar ratio of lactic acid per amine group (the resistance vs protonation is shown in Figure S4). Each data point in Figure 4 was obtained from a separate test where the exact volume of 10 vol % lactic acid solution was directly added to the pDMAPMAM (1 wt %) and the mixture was stirred for 2 h before resistance was measured. As can be seen in Figure 4, the resistance of the solution decreased from 0.5 to 0.25 MΩ by adding 175 μL of lactic acid (lactic acid/amine = 0.4 mol mol<sup>-1</sup>), with a further gradual increase as more lactic acid was added, reaching 0.4 MΩ at 350 μL of lactic acid (lactic acid/amine = 0.8 mol mol<sup>-1</sup>). In addition, the pH of the solution gradually decreased from 10.1 to 4.63 by the slow addition of lactic acid to reach the lactic acid/amine level of 0.8 mol mol<sup>-1</sup>, which confirmed the protonation of the pDMAPMAM in the presence of lactic acid. This behavior is perfectly aligned with the results obtained for the polymer solution bubbled with CO<sub>2</sub> gas (Figure 3), suggesting that: (i) protonation defines the response of pDMAPMAM to CO<sub>2</sub>, and (ii) the impact of protonation on electrical resistance is not trivial.

Considering the final resistance of pDMAPMAM solutions at 100% DOP, the normalized resistance change ( $\Delta R/R_0$ ) can be calculated as a function of pDMAPMAM in the presence of CO<sub>2</sub> (Figure 5). Here, the final DC resistance of solution after exposure to 45 mL min<sup>-1</sup> CO<sub>2</sub> for 60 min was used to calculate  $\Delta R/R_0$ , where  $R_0$  is the initial resistance of the solution. By increasing the pDMAPMAM concentration from 0 to 5 wt %, the total number of CO<sub>2</sub>-responsive moieties in the solution increased, demonstrating an increase in  $\Delta R/R_0$  from 0.73 to

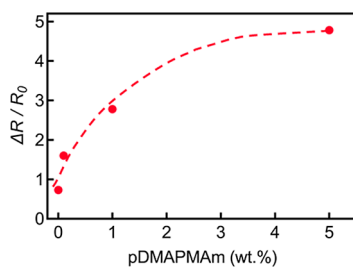


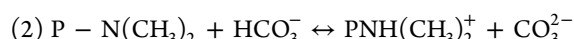
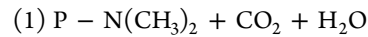
**Figure 5.** Change in normalized resistance as a function of polymer concentration in pDMAPMAM aqueous solutions.

4.78. The raw data for the DOP and resistance of 0, 0.1, 1, and 5 wt % (pDMAPMAM: water) solutions over time can be seen in Figure S5.

**Solid-State Sensing Mechanism Model.** Given that the resistance of the pDMAPMAM solution changes with DOP, we were interested in investigating the behavior of pDMAPMAM in the solid state for the chemiresistive detection of CO<sub>2</sub>. For this purpose, pDMAPMAM ink (pDMAPMAM: ethanol 20 wt %) was printed between two silver electrodes. The SEM images were taken from the top and cross-sectional views to assess the uniformity and homogeneity of the 3D-printed pDMAPMAM films. As shown in Figure 6, the polymer (pDMAPMAM) is uniformly distributed on the substrate. Interestingly, the polymer surface is smoother than the printed silver electrodes. In addition, Figure 6c,d shows that the contact between the polymer and the silver electrodes was optimal for electrical measurements.

A sketch of the sensing mechanism for such a configuration is shown in Figure 7. When gaseous CO<sub>2</sub> (CO<sub>2</sub>(g)) is introduced to the surroundings of the CO<sub>2</sub>-responsive polymer, it dissolves in the water present in the polymer matrix to form solvated carbon dioxide, denoted as CO<sub>2</sub>(aq). The interaction between the pDMAPMAM chains and

solvated CO<sub>2</sub> is based on acid-base chemistry. CO<sub>2</sub>(g) first dissolves in water to form CO<sub>2</sub>(aq), which then reacts with water to form carbonic acid, H<sub>2</sub>CO<sub>3</sub>(aq). The carbonic acid then reacts with the tertiary amine groups of solvated pDMAPMAM generating one bicarbonate (HCO<sub>3</sub><sup>-</sup>(aq)) ion per tertiary amine along the polymer chain



The resultant protonation of the polymer influences the electrical conductivity of the pDMAPMAM.

**CO<sub>2</sub> Responsivity of the Fabricated Polymer (Solid State).** The impact of humidity on the resistance of pDMAPMAM is shown in Figure 8. While a dry pDMAPMAM film was highly resistive (1280 MΩ), the resistance decreased significantly to 12 MΩ at RH = 65% before plateauing for values of RH > 70%. Therefore, all the experiments in the solid state were conducted at RH ≥ 95% to eliminate the impact of humidity on measurements.

The surface morphology and roughness of the pDMAPMAM film in the absence and presence of CO<sub>2</sub> were determined by AFM measurements, as shown in Figure 9. The pDMAPMAM film has a smoother surface with an average roughness of 22.7 nm before CO<sub>2</sub> exposure (Figure 9a,b) while after treatment with CO<sub>2</sub>, the average surface roughness increased to 50.8 nm (Figure 9c,d). The reason for this observation is the CO<sub>2</sub>-responsivity of pDMAPMAM where the tertiary amine sites of pDMAPMAM react with CO<sub>2</sub> in the presence of water, leading to protonation of tertiary amine ligands. The positively charged amine groups repel each other and also facilitate the localized swelling of pDMAPMAM, resulting in a rougher surface.<sup>45</sup>

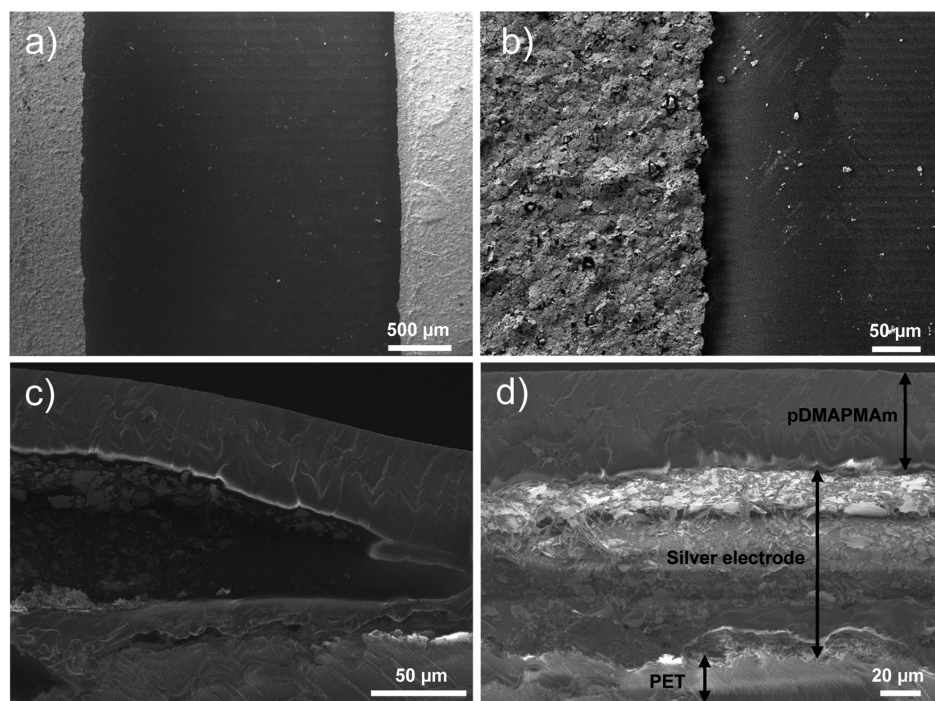


**Figure 6.** SEM images of pDMAPMAM at different magnifications of 500, 50, and 20  $\mu\text{m}$  from (a,b) top and (c,d) cross-sectional views.

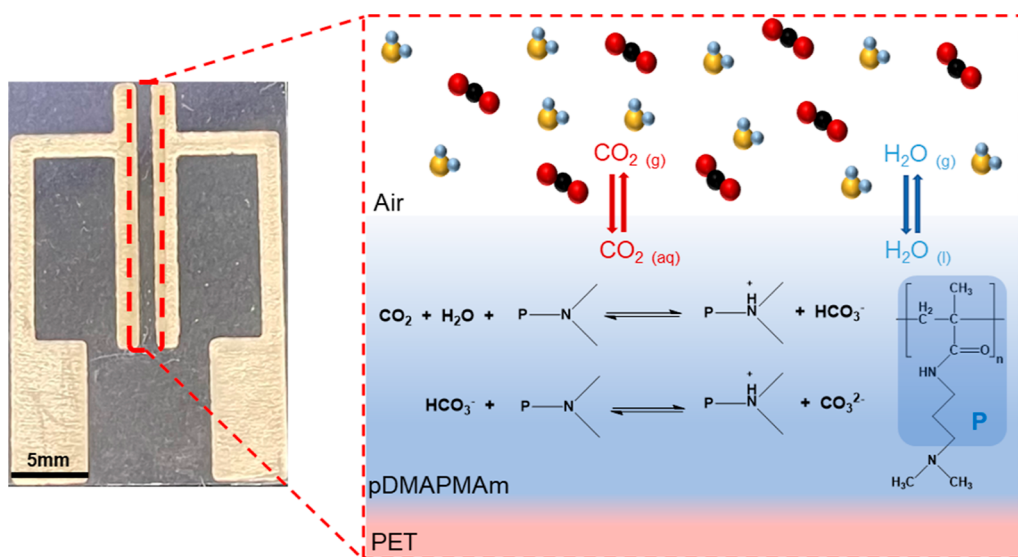


**Figure 7.** Schematic of sensing mechanism. pDMAPMAM (P) was 3D-printed between two silver electrodes on a PET substrate. The  $\text{CO}_2$  and the humidity from air induce the protonation of the polymer, resulting in a change in electrical resistance between the two electrodes.

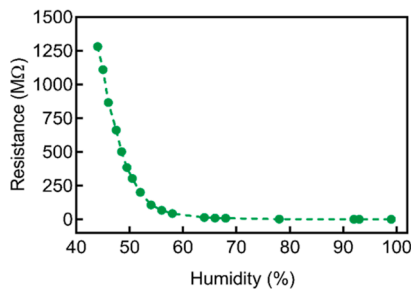


**Figure 8.** Relationship between the resistance of pDMAPMAM films and RH in the solid state.

To explore the surface charge and the surface electrical properties of the pDMAPMAM film in response to  $\text{CO}_2$ , surface potential distribution was obtained by KPFM. As shown in Figure 10, the contact potential difference (CPD) between the tip and the surface of the polymer was  $-600$  and  $640$  mV before and after exposure to  $\text{CO}_2$ , respectively. Therefore, the surface potential has increased by  $+1.24$  V as a result of  $\text{CO}_2$  exposure. This increase is attributed to the accumulation of surface positive charges due to the protonation of pDMAPMAM's tertiary amine sites.<sup>24,46</sup>

The electrical response of pDMAPMAM to extended exposure to  $\text{CO}_2$  in the solid state was studied. For this purpose, the 3D-printed system (a thin film of pDMAPMAM along with the conductive silver electrodes) was exposed to different concentrations of  $\text{CO}_2$  (Figure 11). Figure 11a shows an example of the electrical resistance of pDMAPMAM in the presence of  $10$  vol %  $\text{CO}_2$  (data for  $\text{CO}_2$  concentrations ranging between  $1$  and  $100$  vol % are shown in Figure S6a). Interestingly, continuous exposure of pDMAPMAM solid-state films to  $\text{CO}_2$  gas produced resistance responses similar to those of pDMAPMAM solutions (Figure 3), though much more slowly. Regardless of the concentration of  $\text{CO}_2$ , the resistance of the pDMAPMAM films gradually decreased until a minimum was reached, beyond which resistance increased with time and eventually plateaued at  $\sim 1.25\text{ M}\Omega$ . As observed, pDMAPMAM behaves similar to other reported  $\text{CO}_2$ -responsive polymers such as pDEAEMA<sup>47</sup> and pDMAEMA<sup>48</sup>.

in short-term exposure to  $\text{CO}_2$ . This behavior, however, will change over a longer exposure time demonstrating the importance of this factor on the response of AFPs. The normalized resistance change of pDMAPMAM films ( $\Delta R/R_0$ ) in response to various concentrations of  $\text{CO}_2$  (ranging from  $1$  to  $100$  vol %) is shown in Figure 8b.  $\Delta R$  is defined as  $R_f - R_0$ , where  $R_f$  and  $R_0$  are the final resistance (long term) and initial value, respectively. Interestingly, two distinct behaviors were observed for low and high concentrations of  $\text{CO}_2$ . For the concentrations below  $10$  vol %  $\text{CO}_2$  (region 1, R1), the normalized signal increased continuously to approach a peak of  $20$  vol %. However, at concentrations above  $10$  vol %  $\text{CO}_2$  (region 2, R2), there was a slight drop in normalized resistance. Figure S6b illustrates the correlation between the response time of the pDMAPMAM and the concentration of  $\text{CO}_2$ .

Although it is known that tertiary amines deprotonate when exposed to  $\text{N}_2$  at ambient temperature,<sup>49</sup> the reversibility of polymers occasionally necessitates higher temperatures.<sup>18,34,48</sup> Darabi et al., for example, reported  $\text{CO}_2$ -switchable latexes employing DMAPMAM, which could be redispersed by bubbling  $\text{CO}_2$  at room temperature, whereas the reverse reaction (the desorption of  $\text{CO}_2$  and the deprotonation of tertiary amine sites) needed a higher temperature ( $65^\circ\text{C}$ ) in addition to the  $\text{N}_2$  bubbling.<sup>34</sup> We explored the absorption and desorption of  $\text{CO}_2$  by pDMAPMAM in the solid state via the QCM.<sup>50</sup> In this case, the deposited thin film of pDMAPMAM on the quartz sensor was placed in the QCM cell, and the target gases were passed through the system in three cycles at room temperature as follows:  $\text{N}_2$  with a flow of  $5\text{ mL min}^{-1}$  for  $45$  min,  $\text{CO}_2$  with a flow of  $5\text{ mL min}^{-1}$  for  $1$  h, and  $\text{N}_2$  with a flow of  $5\text{ mL min}^{-1}$  for  $45$  min. As demonstrated in Figure 12a, the frequency values decreased considerably from  $-1.76\text{ Hz}$  to  $-51.74\text{ Hz}$  over time in the presence of  $\text{CO}_2$ , confirming the mass increase of the specimen due to the  $\text{CO}_2$  absorption. Consequently, this  $\text{CO}_2$  absorption affects the extent of protonation and the electrical properties of the polymer (Figures 9, 10b, and S5). The mass increase resulting from  $\text{CO}_2$  absorption appears to be irreversible at room temperature as switching the gas back to  $\text{N}_2$  did not result in a significant

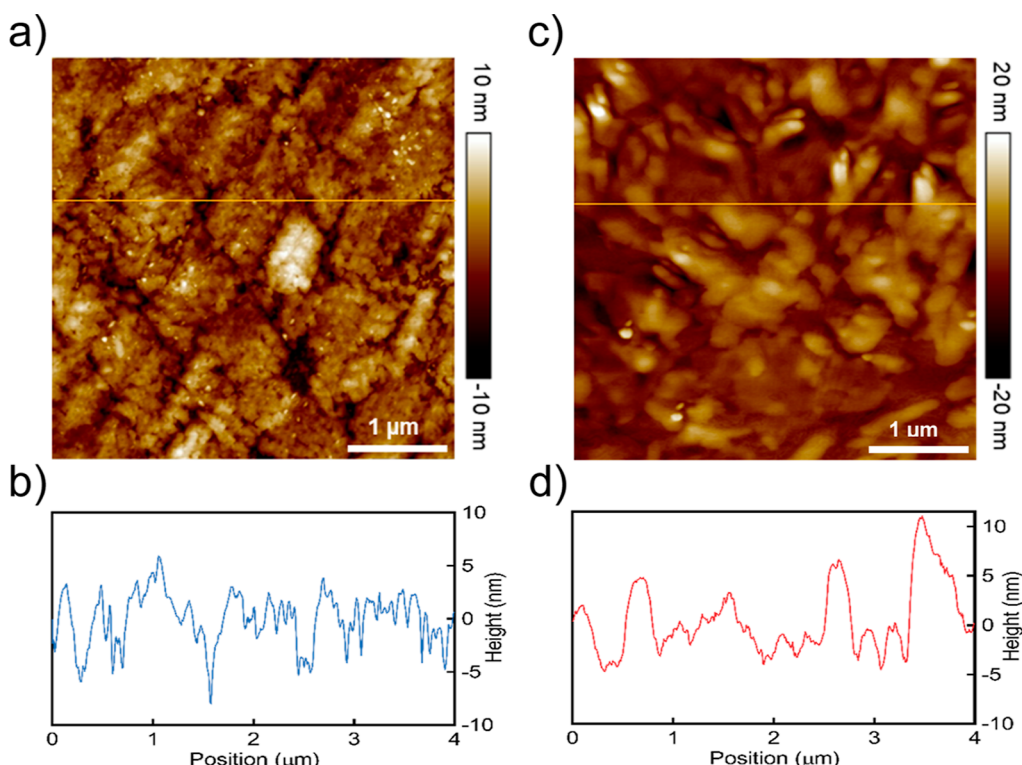


**Figure 9.** AFM topography images and roughness profiles (along the yellow lines) of the pDMPAMAm film before (a,b) and after (c,d) exposure to CO<sub>2</sub>.

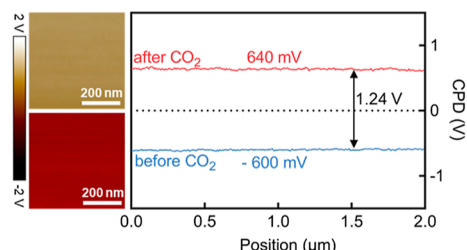


**Figure 10.** KPFM images (left) and the surface potential distribution (right) of the pDMPAMAm film before and after exposure to CO<sub>2</sub>.

increase in frequency values ( $\Delta f = 10$  Hz). In the same direction, a reversibility test was carried out using our in-house

experimental setup (Figure S1). The fabricated polymer-based sensor was placed inside the test chamber, and the target gases were passed through the system in three cycles at room temperature as follows: N<sub>2</sub> with a flow of 10 mL min<sup>-1</sup> for 1 h, CO<sub>2</sub> with a flow of 10 mL min<sup>-1</sup> for 1 h, and N<sub>2</sub> with a flow of 10 mL min<sup>-1</sup> for 1 h. The resistance change of pDMPAMAm is shown in Figure 12b. According to the reversibility result, the observed response of pDMPAMAm to CO<sub>2</sub> is similar to those observed in Figures 11 and S6. However, no significant change in resistance was observed by switching the gas back to N<sub>2</sub>, showing the irreversibility of the CO<sub>2</sub> absorption at room temperature confirming the result of QCM.

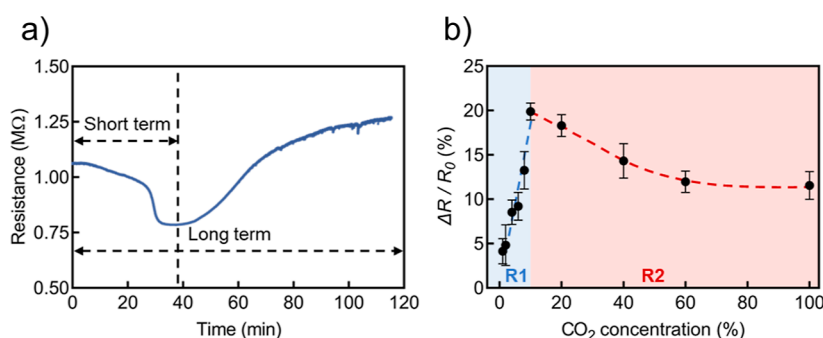


**Figure 11.** Electrical response of pDMPAMAm in the solid state upon continuous exposure to CO<sub>2</sub> for an extended time. (a) Resistance change of the fabricated sensor on exposure to a concentration of 10 vol % CO<sub>2</sub> versus time. The initial decrease in resistance of the pDMPAMAm films over time is denoted here as the “short-term” response of the sensor, while the overall response of the pDMPAMAm films over the whole course of experiments until the final plateau is reached is denoted as “long-term”. (b) Correlation between normalized resistance changes and the concentration of CO<sub>2</sub>. Region 1 (R1) and region 2 (R2) are defined for CO<sub>2</sub> concentrations below and above 10 vol %, respectively. Experiments were repeated three times and standard deviations were estimated at each CO<sub>2</sub> concentration.

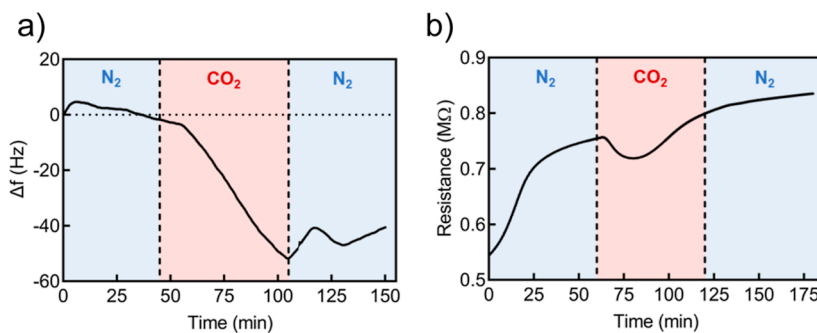


**Figure 12.** Absorption of CO<sub>2</sub> on pDMAPMAM. (a) Frequency change using QCM and (b) resistance change of pDMAPMAM on exposure to N<sub>2</sub> and CO<sub>2</sub>.

## DISCUSSION

The electrical response of pDMAPMAM to extended exposure to CO<sub>2</sub>, both in aqueous solutions and solid state, is intriguing. The DC resistance first decreases until a minimum is reached, and then, with further exposure to CO<sub>2</sub>, the resistance increases, eventually flattening off at a maximum. The rate by which this process takes place depends strongly on the state of the polymer (Figures 3a and 11a). In the liquid phase, where the polymer chains are highly mobile and rapid phase transfer enhances the interaction between CO<sub>2</sub> and amine side groups, the point of minimum resistance appears after 4 min. In contrast, for the solid-state samples, the minimum resistance occurs after 30 min. This trend is irrespective of CO<sub>2</sub> concentration (the solid-state experiments) and pDMAPMAM concentration (aqueous solutions). This observation may have an important practical implication for the design of CO<sub>2</sub> sensors based on AFPs. In a short-term experimental window, the resistance appears to decrease with CO<sub>2</sub>, while over extended periods, the resistance of the same system increases with further exposure to CO<sub>2</sub>. Furthermore, the relationship between the final resistance and CO<sub>2</sub> concentration is curious. While at all CO<sub>2</sub> concentrations that were evaluated (1–100 vol %), the resistance of pDMAPMAM films exceeded their initial resistance after 2 h of exposure, the amplitude by which this increase occurred followed different trends depending on the concentration of CO<sub>2</sub> (Figure 11b). The peak (maximum) that appeared in the normalized resistance change of pDMAPMAM films as a function of CO<sub>2</sub> concentration (Figure 11b) suggests that there may be two competing mechanisms at work. The downward to the upward shift in going from short term to long term in response to CO<sub>2</sub> can be described by proton hopping, the dominant conductivity mechanism in polymers. For example, Lanssegues et al.<sup>51</sup> and Iwase et al.<sup>52</sup> reported that PEI can behave as a solid proton conductor even under anhydrous conditions due to proton hopping. The conductivity of AFPs (e.g., PEI) is highly dependent on the level of protonation and the pK<sub>aH</sub> of the protonated species present in the matrix. Sakurai et al. used branched PEI as a model AFP with all three forms of amine side groups (i.e., primary, secondary, and tertiary).<sup>53</sup> They found a complex trend in the conductivity of PEI when phosphoric acid was used for protonation: by increasing the level of protonation, the conductivity first increases, then decreases, and again increases, revealing three distinct “zones” (Figure 13a). The initial increase in conductivity (Figure 13a, zone 1) is related to a gradual increase in the ratio of protonated to unprotonated amines. In this zone, the level of protonation is still very low, with the limited protonated

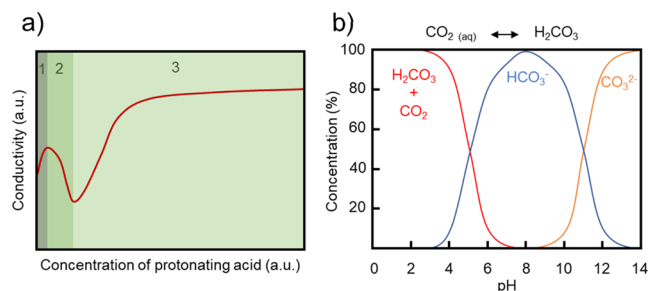


**Figure 13.** (a) Schematic representation of conductivity as a function of protonating acid concentration. The graph was reproduced from data presented in ref 53. (b) schematic representation of concentrations of CO<sub>2</sub>, H<sub>2</sub>CO<sub>3</sub>, HCO<sub>3</sub><sup>-</sup>, and CO<sub>3</sub><sup>2-</sup> over pH 0 to 14. Note that solvated CO<sub>2</sub> is in equilibrium with H<sub>2</sub>CO<sub>3</sub>.

amines still providing suitable sites for proton exchange with their neighboring unprotonated amines. Thus, as the number of protonated sites increases with DOP, so does the conductivity. By further increasing the level of protonation, however, at some point the number of protonated amines considerably exceeds that of unprotonated amines, limiting the possibility of proton hopping. After this stage, conductivity decreases with protonation until all remaining unprotonated amine groups are protonated (Figure 13a, zone 2). Yet again, conductivity is increased by the addition of more protonating species (phosphoric acid in Sakurai’s work) because of proton transfer between unprotonated and protonated solvated acid molecules (Figure 13a, zone 3). In the present study, this process takes place between [H<sub>2</sub>CO<sub>3</sub>(aq) + CO<sub>2</sub>(aq)] molecules (pK<sub>aH</sub> = 6.4) and HCO<sub>3</sub><sup>-</sup> anions (pK<sub>aH</sub> = 10.2). Of note, HCO<sub>3</sub><sup>-</sup> is the dominant anionic species in the pH range from ~6 to ~10 (Figure 13b), providing suitable sites for proton exchange with H<sub>2</sub>CO<sub>3</sub> and CO<sub>2</sub>. Further addition of CO<sub>2</sub> to the system results in the saturation of [H<sub>2</sub>CO<sub>3</sub>(aq) + CO<sub>2</sub>(aq)] (the proton source), leading to an increase in conductivity (or continuous decrease in resistance). The practical translation of these two competing processes led to the appearance of the peak in resistance as a function of CO<sub>2</sub> concentration.

The impact of protonation on the response of pDMAPMAM to CO<sub>2</sub> exposure was further investigated by first pre-treating pDMAPMAM ink with dilute HCl. The ink was then cast between silver electrodes and, after drying, the film was placed in a humidified chamber (RH ≥ 95%), and CO<sub>2</sub> gas was introduced. Unlike the usual response of pDMAPMAM films to CO<sub>2</sub> gas over time in which resistance first decreased and then increased (Figure 11a), the DC resistance of partially protonated films simply continued to rise (no downward

"trough" was observed) (Figures 14 and S7). This behavior resembles the second part of the untreated pDMAPMAM

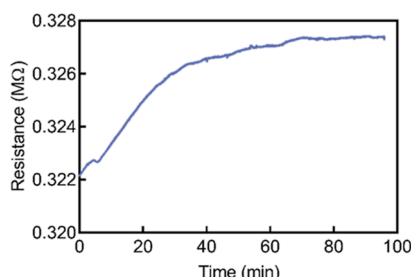


**Figure 14.** Resistance of a pDMAPMAM film pre-treated with HCl. CO<sub>2</sub> was introduced (RH ≥ 95%) at time = 0.

film's response to CO<sub>2</sub>, suggesting that the initial reduction in resistance originates from the initial protonation of the pDMAPMAM chains at the early stages of protonation.

## CONCLUSIONS

In this study, pDMAPMAM decorated with tertiary amine side groups and a  $pK_{aH}$  higher than most reported CO<sub>2</sub>-switchable polymers is synthesized by free radical polymerization to explore its electrical response to CO<sub>2</sub> in both aqueous and solid phases. The high  $pK_{aH}$  value of the polymer guarantees that pDMAPMAM is protonated in the presence of CO<sub>2</sub> over a wide pH range. It is found that the DC resistance of pDMAPMAM in both the aqueous and solid phases is impacted by the level of humidity, CO<sub>2</sub> concentration in the surrounding environment, and duration of exposure to CO<sub>2</sub>. In the liquid phase, the key factor is the concentration of pDMAPMAM. Unlike most CO<sub>2</sub>-responsive sensors whose resistance decreases over time, in this study, the DC resistance of pDMAPMAM demonstrates an interesting and unique behavior in both the aqueous and solid phases. The resistance of pDMAPMAM decreased during the early stages of exposure to CO<sub>2</sub> and then increased over time in both phases; however, this behavior change occurs much more slowly in the solid state compared to the aqueous phase. The change in resistance versus CO<sub>2</sub> concentration is first positive and then negative, suggesting the presence of two competing mechanisms: an increase in resistance due to over-protonation of amine groups on the polymer and a reduction in resistance due to the saturation of the system with H<sub>2</sub>CO<sub>3</sub>. This study, for the first time, provides a better understanding of the electrical response of pDMAPMAM as a model CO<sub>2</sub>-responsive polymer to extended exposure to CO<sub>2</sub>. Our results show that the electrical behavior of pDMAPMAM is a function of the DOP. At a low DOP (<50%), where the amine side groups are largely unprotonated, the resistance decreases as the number of protonated amines increases. Yet, when the protonated amine side groups dominate in the system, proton hopping between protonated and unprotonated amine groups is disrupted, leading to a gradual increase in resistance. The time-dependent response of this polymer may not be a concern for the applications such as CO<sub>2</sub> capture; however, tuning the structure of this polymer to have a polymeric system with a robust electrical response is critical to enabling reliable CO<sub>2</sub> sensing over a wide range of concentrations.

## ASSOCIATED CONTENT

### Supporting Information

The Supporting Information is available free of charge at <https://pubs.acs.org/doi/10.1021/acsomega.2c00914>.

Experimental setup, protonation of polymer solution in the presence of CO<sub>2</sub>, resistance of polymer solution as a function of pH and protonation, and electrical response of polymer films to CO<sub>2</sub> ([PDF](#))

## AUTHOR INFORMATION

### Corresponding Authors

**Fariba Dehghani** – School of Chemical and Biomolecular Engineering, The University of Sydney, Sydney, NSW 2006, Australia; The University of Sydney, Sydney Nano Institute, NSW 2006, Australia; orcid.org/0000-0002-7805-8101; Email: [fariba.dehghani@sydney.edu.au](mailto:fariba.dehghani@sydney.edu.au)

**Sina Naficy** – School of Chemical and Biomolecular Engineering, The University of Sydney, Sydney, NSW 2006, Australia; orcid.org/0000-0001-9168-6746; Email: [sina.naficy@sydney.edu.au](mailto:sina.naficy@sydney.edu.au)

### Authors

**Zahra Shahrabaki** – School of Chemical and Biomolecular Engineering, The University of Sydney, Sydney, NSW 2006, Australia

**Farshad Oveissi** – School of Chemical and Biomolecular Engineering, The University of Sydney, Sydney, NSW 2006, Australia; orcid.org/0000-0002-7464-8251

**Syamak Farajikhah** – School of Chemical and Biomolecular Engineering, The University of Sydney, Sydney, NSW 2006, Australia; The University of Sydney, Sydney Nano Institute, NSW 2006, Australia; orcid.org/0000-0002-2997-5931

**Mohammad B. Ghasemian** – School of Chemical Engineering, University of New South Wales (UNSW), Sydney, NSW 2052, Australia; orcid.org/0000-0002-5618-0106

**Ross D. Jansen-van Vuuren** – Faculty of Chemistry and Chemical Technology, University of Ljubljana, 1000 Ljubljana, Slovenia; orcid.org/0000-0002-2919-6962

**Philip G. Jessop** – Department of Chemistry, Queen's University, Kingston, Ontario K7L 3N6, Canada

**Jimmy Yun** – School of Chemical Engineering, University of New South Wales (UNSW), Sydney, NSW 2052, Australia; Qingdao International Academician Park Research Institute, Qingdao, Shandong 266104, PR China

Complete contact information is available at:

<https://pubs.acs.org/10.1021/acsomega.2c00914>

### Notes

The authors declare no competing financial interest.

## ACKNOWLEDGMENTS

The authors acknowledge the financial support provided by the Australian Research Council (ARC Linkage Project LP180100309) and the Centre for Advanced Food Engineering (CAFE) at the University of Sydney. The authors thank Karen Hakobyan and Ronil J. Rath for their assistance in, respectively, SEC and QCM analysis. F.O. acknowledges the financial support by the School of Chemical and Biomolecular Engineering at the University of Sydney for his F.H. Loxton Postdoctoral Research Fellowship.

## ■ ABBREVIATIONS

<sup>1</sup>H NMR, proton nuclear magnetic resonance; AFM, atomic force microscopy; AFPs, amine-functionalized polymers; AIBN, 2,2'-azobis(2-methylpropionitrile); CPD, contact potential difference; DC, direct current; DMAc, *N,N*-dimethylacetamide; DOP, degree of protonation; FTIR, Fourier-transform infrared spectroscopy; HCl, hydrochloric acid; KPFM, Kelvin probe force microscopy; Mw, molecular weight; pDEAEMA, poly(*N,N*-diethylaminoethyl methacrylate); pDMAEMA, poly(*N,N*-dimethylaminoethyl methacrylate); pDAMPAm, poly(*N*-[3-(dimethylamino)propyl] methacrylamide); PEI, polyethyleneimine; PET, polyethylene terephthalate; QCM, quartz crystal microbalance; RH, relative humidity; SEC, size exclusion chromatography; SEM, scanning electron microscopy

## ■ REFERENCES

- (1) (a) Molina, A.; Escobar-Barrios, V.; Oliva, J. A review on hybrid and flexible CO<sub>2</sub> gas sensors. *Synth. Met.* **2020**, *270*, 116602. (b) Dervieux, E.; Théron, M.; Uhrling, W. Carbon Dioxide Sensing—Biomedical Applications to Human Subjects. *Sensors* **2021**, *22*, 188.
- (c) Zhou, X.; Lee, S.; Xu, Z.; Yoon, J. Recent progress on the development of chemosensors for gases. *Chem. Rev.* **2015**, *115*, 7944–8000. (d) Neethirajan, S.; Jayas, D. S.; Sadistap, S. Carbon Dioxide (CO<sub>2</sub>) Sensors for the Agri-food Industry—A Review. *Food Bioprocess Technol.* **2009**, *2*, 115–121.
- (2) (a) Singh, O. P.; Howe, T. A.; Malarvili, M. Real-time human respiration carbon dioxide measurement device for cardiorespiratory assessment. *J. Breath Res.* **2018**, *12*, 026003. (b) Nasiri, N.; Clarke, C. Nanostructured chemiresistive gas sensors for medical applications. *Sensors* **2019**, *19*, 462.
- (3) (a) Jiang, C.; Masood, M. K.; Soh, Y. C.; Li, H. Indoor occupancy estimation from carbon dioxide concentration. *Energy Build.* **2016**, *131*, 132–141. (b) Wang, H.; Vagin, S. I.; Rieger, B.; Meldrum, A. An Ultrasensitive Fluorescent Paper-Based CO<sub>2</sub> Sensor. *ACS Appl. Mater. Interfaces* **2020**, *12*, 20507–20513.
- (4) (a) Neurauter, G.; Klimant, I.; Wolfbeis, O. S. Fiber-optic microsensor for high resolution pCO<sub>2</sub> sensing in marine environment. *Fresenius. J. Anal. Chem.* **2000**, *366*, 481–487. (b) Fritzsche, E.; Gruber, P.; Schutting, S.; Fischer, J. P.; Strobl, M.; Müller, J. D.; Borisov, S. M.; Klimant, I. Highly sensitive poisoning-resistant optical carbon dioxide sensors for environmental monitoring. *Anal. Methods* **2017**, *9*, 55–65.
- (5) Chen, S.-J.; Hovde, D. C.; Peterson, K. A.; Marshall, A. W. Fire detection using smoke and gas sensors. *Fire Saf. J.* **2007**, *42*, 507–515.
- (6) Soltani Firouz, M.; Mohi-Alden, K.; Omid, M. A critical review on intelligent and active packaging in the food industry: Research and development. *Food Res. Int.* **2021**, *141*, 110113.
- (7) Puligundla, P.; Jung, J.; Ko, S. Carbon dioxide sensors for intelligent food packaging applications. *Food Control* **2012**, *25*, 328–333.
- (8) (a) Yu, L.; Li, Y.; Yu, H.; Zhang, K.; Wang, X.; Chen, X.; Yue, J.; Huo, T.; Ge, H.; Alamry, K. A.; Marwani, H. M.; Wang, S. A fluorescence probe for highly selective and sensitive detection of gaseous ozone based on excited-state intramolecular proton transfer mechanism. *Sens. Actuators, B* **2018**, *266*, 717–723. (b) Yan, Y.; Zhang, K.; Yu, H.; Zhu, H.; Sun, M.; Hayat, T.; Alsaedi, A.; Wang, S. Sensitive detection of sulfide based on the self-assembly of fluorescent silver nanoclusters on the surface of silica nanospheres. *Talanta* **2017**, *174*, 387–393. (c) Sun, M.; Yu, H.; Zhang, K.; Wang, S.; Hayat, T.; Alsaedi, A.; Huang, D. Palladacycle based fluorescence turn-on probe for sensitive detection of carbon monoxide. *ACS Sens.* **2018**, *3*, 285–289.
- (9) Bulbul, A.; Kim, H. A bubble-based microfluidic gas sensor for gas chromatographs. *Lab Chip* **2015**, *15*, 94–104.
- (10) Dinh, T.-V.; Choi, I.-Y.; Son, Y.-S.; Kim, J.-C. A review on non-dispersive infrared gas sensors: Improvement of sensor detection limit and interference correction. *Sens. Actuators, B* **2016**, *231*, 529–538.
- (11) Borchert, N. B.; Kerry, J. P.; Papkovsky, D. B. A CO<sub>2</sub> sensor based on Pt-porphyrin dye and FRET scheme for food packaging applications. *Sens. Actuators, B* **2013**, *176*, 157–165.
- (12) Zhai, X.; Li, Z.; Shi, J.; Huang, X.; Sun, Z.; Zhang, D.; Zou, X.; Sun, Y.; Zhang, J.; Holmes, M.; Gong, Y.; Povey, M.; Wang, S. A colorimetric hydrogen sulfide sensor based on gellan gum-silver nanoparticles bionanocomposite for monitoring of meat spoilage in intelligent packaging. *Food Chem.* **2019**, *290*, 135–143.
- (13) (a) Zhang, Y.; Lim, L.-T. Colorimetric array indicator for NH<sub>3</sub> and CO<sub>2</sub> detection. *Sens. Actuators, B* **2018**, *255*, 3216–3226. (b) Rukchon, C.; Nopwinyuwong, A.; Trevanich, S.; Jinkarn, T.; Suppakul, P. Development of a food spoilage indicator for monitoring freshness of skinless chicken breast. *Talanta* **2014**, *130*, 547–554. (c) Nopwinyuwong, A.; Trevanich, S.; Suppakul, P. Development of a novel colorimetric indicator label for monitoring freshness of intermediate-moisture dessert spoilage. *Talanta* **2010**, *81*, 1126–1132. (d) Perez de Vargas-Sansalvador, I. M.; Erenas, M. M.; Diamond, D.; Quilty, B.; Capitan-Vallvey, L. F. Water based-ionic liquid carbon dioxide sensor for applications in the food industry. *Sens. Actuators, B* **2017**, *253*, 302–309.
- (14) Hong, H. S.; Kim, J. W.; Jung, S. J.; Park, C. O. Thick Film Planar CO<sub>2</sub> Sensors Based on Na  $\beta$ -Alumina Solid Electrolyte. *J. Electroceram.* **2005**, *15*, 151–157.
- (15) Dincer, C.; Bruch, R.; Costa-Rama, E.; Fernández-Abedul, M. T.; Merkoçi, A.; Manz, A.; Urban, G. A.; Güder, F. Disposable sensors in diagnostics, food, and environmental monitoring. *Adv. Mater.* **2019**, *31*, 1806739.
- (16) Zerger, A.; Viscarra Rossel, R. A.; Swain, D. L.; Wark, T.; Handcock, R. N.; Doerr, V. A. J.; Bishop-Hurley, G. J.; Doerr, E. D.; Gibbons, P. G.; Lobsey, C. Environmental sensor networks for vegetation, animal and soil sciences. *Int. J. Appl. Earth Obs. Geoinf.* **2010**, *12*, 303–316.
- (17) (a) Zhang, Q.; Yu, G.; Wang, W.-J.; Li, B.-G.; Zhu, S. Preparation of CO<sub>2</sub>/N<sub>2</sub>-Triggered Reversibly Coagulatable and Redispersible Polyacrylate Latexes by Emulsion Polymerization Using a Polymeric Surfactant. *Macromol. Rapid Commun.* **2012**, *33*, 916–921. (b) Lin, S.; Theato, P. CO<sub>2</sub>-Responsive Polymers. *Macromol. Rapid Commun.* **2013**, *34*, 1118–1133.
- (18) Pinaud, J.; Kowal, E.; Cunningham, M.; Jessop, P. 2-(Diethyl)aminoethyl Methacrylate as a CO<sub>2</sub>-Switchable Comonomer for the Preparation of Readily Coagulated and Redispersed Polymer Latexes. *ACS Macro Lett.* **2012**, *1*, 1103–1107.
- (19) Yan, Q.; Zhou, R.; Fu, C.; Zhang, H.; Yin, Y.; Yuan, J. CO<sub>2</sub>-Responsive Polymeric Vesicles that Breathe. *Angew. Chem., Int. Ed.* **2011**, *50*, 4923–4927.
- (20) Guo, Z.; Feng, Y.; Wang, Y.; Wang, J.; Wu, Y.; Zhang, Y. A novel smart polymer responsive to CO<sub>2</sub>. *Chem. Commun.* **2011**, *47*, 9348–9350.
- (21) Quek, J. Y.; Davis, T. P.; Lowe, A. B. Amidine functionality as a stimulus-responsive building block. *Chem. Soc. Rev.* **2013**, *42*, 7326–7334.
- (22) Quek, J. Y.; Roth, P. J.; Evans, R. A.; Davis, T. P.; Lowe, A. B. Reversible addition-fragmentation chain transfer synthesis of amidine-based, CO<sub>2</sub>-responsive homo and AB diblock (Co)polymers comprised of histamine and their gas-triggered self-assembly in water. *J. Polym. Sci., Part A: Polym. Chem.* **2013**, *51*, 394–404.
- (23) Liu, H.; Zhao, Y.; Dreiss, C. A.; Feng, Y. CO<sub>2</sub>-switchable multi-compartment micelles with segregated corona. *Soft Matter* **2014**, *10*, 6387–6391.
- (24) Yan, Q.; Zhao, Y. CO<sub>2</sub>-Stimulated Diversiform Deformations of Polymer Assemblies. *J. Am. Chem. Soc.* **2013**, *135*, 16300–16303.
- (25) Liu, H.; Lin, S.; Feng, Y.; Theato, P. CO<sub>2</sub>-responsive polymer materials. *Polym. Chem.* **2017**, *8*, 12–23.
- (26) Alshamrani, A. K.; Vanderveen, J. R.; Jessop, P. G. A guide to the selection of switchable functional groups for CO<sub>2</sub>-switchable compounds. *Phys. Chem. Chem. Phys.* **2016**, *18*, 19276–19288.

- (27) Han, M.; Jung, S.; Lee, Y.; Jung, D.; Kong, S. H. PEI-Functionalized Carbon Nanotube Thin Film Sensor for CO<sub>2</sub> Gas Detection at Room Temperature. *Micromachines* **2021**, *12*, 1053.
- (28) Kainz, J.; Werz, P. D. L.; Troll, C.; Rieger, B. Temperature and CO<sub>2</sub> responsive polyethylenimine for highly efficient carbon dioxide release. *RSC Adv.* **2015**, *5*, 9556–9560.
- (29) Yao, D.; Li, T.; Zheng, Y.; Zhang, Z. Fabrication of a functional microgel-based hybrid nanofluid and its application in CO<sub>2</sub> gas adsorption. *React. Funct. Polym.* **2019**, *136*, 131–137.
- (30) Han, D.; Tong, X.; Boissière, O.; Zhao, Y. General Strategy for Making CO<sub>2</sub>-Switchable Polymers. *ACS Macro Lett.* **2012**, *1*, 57–61.
- (31) Li, X.-Y.; Xie, R.; Luo, F.; Jia, Z.-H.; Shi, K.; Ju, X.-J.; Wang, W.; Liu, Z.; Chu, L.-Y. CO<sub>2</sub>-responsive poly(N,N-dimethylaminoethyl methacrylate) hydrogels with fast responsive rate. *J. Taiwan Inst. Chem. Eng.* **2019**, *94*, 135–142.
- (32) Wang, Y.; Huo, M.; Zeng, M.; Liu, L.; Ye, Q.-Q.; Chen, X.; Li, D.; Peng, L.; Yuan, J.-Y. CO<sub>2</sub>-responsive Polymeric Fluorescent Sensor with Ultrafast Response. *Chin. J. Polym. Sci.* **2018**, *36*, 1321–1327.
- (33) Guo, S.; Zhang, H.; Lu, X.; Xiao, H.; Zhao, Y. Sensing carbon dioxide through a solution transparency change in gas-responsive polymers. *J. Mater. Chem. C* **2019**, *7*, 4049–4056.
- (34) Darabi, A.; Glasing, J.; Jessop, P. G.; Cunningham, M. F. Preparation of CO<sub>2</sub>-switchable latexes using N-[3-(dimethylamino)-propyl]-methacrylamide (DMAPMAM). *J. Polym. Sci., Part A: Polym. Chem.* **2017**, *55*, 1059–1066.
- (35) Fowler, C. I.; Jessop, P. G.; Cunningham, M. F. Aryl amidine and tertiary amine switchable surfactants and their application in the emulsion polymerization of methyl methacrylate. *Macromolecules* **2012**, *45*, 2955–2962.
- (36) van de Wetering, P.; Moret, E. E.; Schuurmans-Nieuwenbroek, N. M. E.; van Steenbergen, M. J.; Hennink, W. E. Structure–Activity Relationships of Water-Soluble Cationic Methacrylate/Methacrylamide Polymers for Nonviral Gene Delivery. *Bioconjug. Chem.* **1999**, *10*, 589–597.
- (37) (a) Jing, X.; Lu, H.; Wang, B.; Huang, Z. CO<sub>2</sub>-switchable polymeric vesicle-network structure transition induced by a hairpin-line molecular configuration conversion. *J. Appl. Polym. Sci.* **2017**, *134*, 44417. (b) Liu, H.; Yin, H.; Feng, Y. A CO<sub>2</sub>-switchable amidine monomer: synthesis and characterization. *Des. Monomers Polym.* **2017**, *20*, 363–367. (c) Jing, X.-W.; Huang, Z.-Y.; Lu, H.-S.; Wang, B.-G. CO<sub>2</sub>-sensitive amphiphilic triblock copolymer self-assembly morphology transition and accelerating drug release from polymeric vesicle. *Chin. J. Polym. Sci.* **2018**, *36*, 18–24. (d) Wang, L.; Zhao, J.; Lu, H.; Huang, Z.; Wang, B. Selective separation of aliphatic tertiary amines and aromatic amines by using CO<sub>2</sub>. *Sep. Purif. Technol.* **2020**, *239*, 116526.
- (38) Doan, T. C. D.; Baggerman, J.; Ramaneti, R.; Tong, H. D.; Marcelis, A. T. M.; van Rijn, C. J. M. Carbon dioxide detection with polyethylenimine blended with polyelectrolytes. *Sens. Actuators, B* **2014**, *201*, 452–459.
- (39) (a) Mishra, R. K.; Ray, A. R. Synthesis and characterization of poly{N-[3-(dimethylamino) propyl] methacrylamide-co-itaconic acid} hydrogels for drug delivery. *J. Appl. Polym. Sci.* **2011**, *119*, 3199–3206. (b) Esselin, N.; Portolan, F.; Domloge, N.; Clark, R. B.; Musa, O. M.; Pilard, J.-F. Offline Monitoring of Hydroxyethyl Methacrylate and 3-Dimethylaminopropyl Methacrylamide Copolymerization: Correlation Between FTIR and GC Quantifications. *Spectrosc. Lett.* **2015**, *48*, 53–58.
- (40) Schmitz, S.; Ritter, H. Access to Poly{N-[3-(dimethylamino)-propyl](meth)acrylamide} via Microwave-Assisted Synthesis and Control of LCST-Behavior in Water. *Macromol. Rapid Commun.* **2007**, *28*, 2080–2083.
- (41) Cunningham, M. F.; Jessop, P. G. An introduction to the principles and fundamentals of CO<sub>2</sub>-switchable polymers and polymer colloids. *Eur. Polym. J.* **2016**, *76*, 208–215.
- (42) Darabi, A.; Jessop, P. G.; Cunningham, M. F. CO<sub>2</sub>-responsive polymeric materials: synthesis, self-assembly, and functional applications. *Chem. Soc. Rev.* **2016**, *45*, 4391–4436.
- (43) Cunningham, M. F.; Jessop, P. G. Carbon dioxide-switchable polymers: where are the future opportunities? *Macromolecules* **2019**, *52*, 6801–6816.
- (44) Jansen-van Vuuren, R. D.; Drechsler Vilela, G.; Ramezani, M.; Gilbert, P. H.; Watson, D.; Mullins, N.; Lucas, A. K.; Giacomini, A. J.; Cunningham, M. F.; Jessop, P. G. CO<sub>2</sub>-responsive superabsorbent hydrogels capable of > 90% dewatering when immersed in water. *ACS Appl. Polym. Mater.* **2021**, *3*, 2153–2165.
- (45) Che, H.; Huo, M.; Peng, L.; Fang, T.; Liu, N.; Feng, L.; Wei, Y.; Yuan, J. CO<sub>2</sub>-Responsive Nanofibrous Membranes with Switchable Oil/Water Wettability. *Angew. Chem., Int. Ed.* **2015**, *127*, 9062–9066.
- (46) Garcia-Valdez, O.; Brescacin, T.; Arredondo, J.; Bouchard, J.; Jessop, P. G.; Champagne, P.; Cunningham, M. F. Grafting CO<sub>2</sub>-responsive polymers from cellulose nanocrystals via nitroxide-mediated polymerisation. *Polym. Chem.* **2017**, *8*, 4124–4131.
- (47) Liu, H.; Guo, Z.; He, S.; Yin, H.; Fei, C.; Feng, Y. CO<sub>2</sub>-driven vesicle to micelle regulation of amphiphilic copolymer: random versus block strategy. *Polym. Chem.* **2014**, *5*, 4756–4763.
- (48) Yin, H.; Bulteau, A.-L.; Feng, Y.; Billon, L. CO<sub>2</sub>-Induced Tunable and Reversible Surface Wettability of Honeycomb Structured Porous Films for Cell Adhesion. *Adv. Mater. Interfaces* **2016**, *3*, 1500623.
- (49) (a) Wang, W.; Liu, H.; Mu, M.; Yin, H.; Feng, Y. CO<sub>2</sub>-induced reversible morphology transition from giant worms to polymersomes assembled from a block-random segmented copolymer. *Polym. Chem.* **2015**, *6*, 2900–2908. (b) Zhang, Y.; Feng, Y.; Wang, Y.; Li, X. CO<sub>2</sub>-Switchable Viscoelastic Fluids Based on a Pseudogemini Surfactant. *Langmuir* **2013**, *29*, 4187–4192.
- (50) (a) Tsionsky, V.; Gileadi, E. Use of the quartz crystal microbalance for the study of adsorption from the gas phase. *Langmuir* **1994**, *10*, 2830–2835. (b) Xie, J.; Zhang, L.; Xing, H.; Bai, P.; Liu, B.; Wang, C.; Lei, K.; Wang, H.; Peng, S.; Yang, S. Gas sensing of ordered and disordered structure SiO<sub>2</sub> and their adsorption behavior based on Quartz Crystal Microbalance. *Sens. Actuators, B* **2020**, *305*, 127479. (c) Berouaken, M.; Yaddadene, C.; Chebaut, K.; Ayat, M.; Menari, H.; Belaid, S.; Gabouze, N. CO<sub>2</sub> Gas Sensors Based on Hydrophilic Vanadium Oxide Thin Film Coated QCM. *CO<sub>2</sub> Gas Sensors Based on Hydrophilic Vanadium Oxide Thin Film Coated QCM*. In ICREEC 2019; Springer, 2020, pp 633–638. DOI: 10.1007/978-981-15-5444-5\_79
- (51) Daniel, M. F.; Desbat, B.; Cruege, F.; Trinquet, O.; Lassegues, J. C. Solid state protonic conductors: Poly(ethylene imine) sulfates and phosphates. *Solid State Ionics* **1988**, 28–30, 637–641.
- (52) Tanaka, R.; Yamamoto, H.; Kawamura, S.; Iwase, T. *Electrochim. Acta* **1995**, *40*, 2421–2424.
- (53) Tanaka, R.; Yamamoto, H.; Shono, A.; Kubo, K.; Sakurai, M. Proton conducting behavior in non-crosslinked and crosslinked polyethylenimine with excess phosphoric acid. *Electrochim. Acta* **2000**, *45*, 1385–1389.